Astronomy & Astrophysics manuscript no. corot12˙v9
June 1, 2010

Transiting exoplanets from the CoRoT space mission⋆

XI. CoRoT-12b: a short-period low-density planet transiting a solar analog star

M. Gillon[1], A. Hatzes[2], Sz. Csizmadia[3], M. Fridlund[4], M. Deleuil[5], S. Aigrain[6], R. Alonso[7], M. Auvergne[8], A. Baglin[8], P. Barge[5], S. I. Barnes[9], A. S. Bonomo[5], P. Bordé[10], F. Bouchy[11,12], J. Cabrera[3,13], L. Carone[14], S. Carpano[4], W. D. Cochran[15], H. J. Deeg[16], R. Dvorak[17], M. Endl[15], A. Erikson[17], S. Ferraz-Mello[18], D. Gandolfi[4], J. C. Gazzano[5], E. Guenther[2], T. Guillot[19], M. Havel[19], G. Hébrard[12], L. Jorda[5], A. Léger[10], A. Llebaria[10], H. Lammer[20], C. Lovis[7], M. Mayor[7], T. Mazeh[21], J. Montalbán[1], C. Moutou[5], A. Ofir[21], M. Ollivier[10], M. Pätzold[14], F. Pepe[7], D. Queloz[7], H. Rauer[3,22], D. Rouan[5], B. Samuel[10], A. Santerne[5], J. Schneider[13], B. Tingley[16], S. Udry[7], J. Weingrill[20], and G. Wuchterl[2]

(Affiliations can be found after the references)

Received date / accepted date

ABSTRACT

We report the discovery by the CoRoT satellite of a new transiting giant planet in a 2.83 days orbit about a V=15.5 solar analog star ($M_* = 1.08 \pm 0.08\ M_\odot$, $R_* = 1.1 \pm 0.1\ R_\odot$, $T_{\rm eff} = 5675 \pm 80$ K). This new planet, CoRoT-12b, has a mass of $0.92 \pm 0.07\ M_{Jup}$ and a radius of $1.44 \pm 0.13\ R_{Jup}$. Its low density can be explained by standard models for irradiated planets.

Key words. stars: planetary systems - star: individual: CoRoT-12 - techniques: photometric - techniques: radial velocities - techniques: spectroscopic

1. Introduction

Because of their special geometric configuration, a wealth of information can be learned about transiting extrasolar planets (e.g., Winn 2010), making them very important for our understanding of the vast planetary population hosted by our galaxy. They are the only exoplanets for which accurate measurements of the mass and radius are available. Furthermore, their atmospheric properties can be studied during their transits and occultations (e.g., Deming & Seager 2009).

More than 70 extrasolar planets transiting their parent stars are now known[1], most of which having been discovered by dedicated photometric surveys. Among these, the CoRoT (Co*nvection*, RO*tation*, *and planetary* T*ransits*) space mission (Baglin et al. 2009) stands out as a pionner project. Because of its excellent instrumental capabilities and its low Earth orbit, CoRoT can monitor the same fields of view with a very high photometric precision for up to five months. This makes possible the detection of planets that would be out of reach for ground-based surveys, as demonstrated for instance by its discovery of the first transiting 'Super-Earth' CoRoT-7b (Léger et al. 2009; Queloz et al. 2009), and the first 'temperate' transiting gaseous planet CoRoT-9b (Deeg et al. 2010).

We report here the discovery of a new planet by CoRoT, a 'hot Jupiter' called CoRoT-12b, that transits a $m_V = 15.5$ solar analog star. We present the CoRoT discovery photometry in Sec. 2. The follow-up ground-based observations establishing the planetary nature of CoRoT-12b are presented in Sec. 3, while the spectroscopic determination of the parameters of the host star is described in Sec. 4. A global Bayesian analysis of the CoRoT and follow-up data is presented with its results in Sec. 5. Finally, we discuss the inferred properties of the CoRoT-12 system in Sec. 6.

2. CoRoT photometric observations

Table 1 presents the ID, coordinates and magnitude of CoRoT-12. This star is located in a field near the galactic anti-center direction, in the *Monoceros* constellation. It was monitored by CoRoT during its run *LRa*01 that took place from October 24, 2007 to March 3, 2008. The particularities of that CoRoT run are described by Rauer et al. (2009) and Carone et al. (in prep.).

The transits of CoRoT-12b were noticed after 29 days by the so-called 'alarm mode' pipeline (Surace et al. 2008). The time-sampling was then changed from 512s, the nominal value, to 32s. The processed light curve (LC) of CoRoT-12 is shown in Fig. 1. This monochromatic LC consists of 258 043 photometric measurements for a total duration of 131 days. It results from the processing of the raw CoRoT measurements by the standard CoRoT pipeline (version 2.1, see Auvergne et al. 2009), followed by a further processing (outliers rejection and systematics correction) similar to what is described by, e.g., Barge et al. (2008) and Alonso et al. (2008). 47 transits of CoRoT-12b are present in the LC, 36 of them being found in its oversampled part. Some discontinuities are present in the LC. They were caused by energetic particles hits during the crossings of the South-Atlantic Anomaly by the satellite. A large jump of the

Send offprint requests to: michael.gillon@ulg.ac.be

⋆ The CoRoT space mission, launched on December 27th 2006, has been developed and is operated by CNES, with the contribution of Austria, Belgium, Brazil , ESA (RSSD and Science Programme), Germany and Spain.

[1] See, e.g., Jean Schneider's Extrasolar Planet Encyclopedia at http://exoplanet.eu

CoRoT window ID	LRa01 E2 3459
CoRoT ID	0102671819
UCAC2 ID	31290403
USNO-A2 ID	0825-03015398
USNO-B1 ID	0887-0101512
2MASS ID	J06430476-0117471
GSC2.3 ID	SB3BK006251
Coordinates	
RA (J2000)	06 43 03.76
Dec (J2000)	-01 17 47.12

Magnitudes

Filter	Mag	Error
B[a]	16.343	0.080
V[a]	15.515	0.052
r'[a]	15.211	0.040
i'[a]	14.685	0.069
J[b]	14.024	0.029
H[b]	13.630	0.030
K[b]	13.557	0.041

[a] Provided by Exo-Dat (Deleuil et al, 2009).
[b] from 2MASS catalog (Skrustkie et al. 2006).

Table 1. IDs, coordinates and magnitudes for the star CoRoT-12.

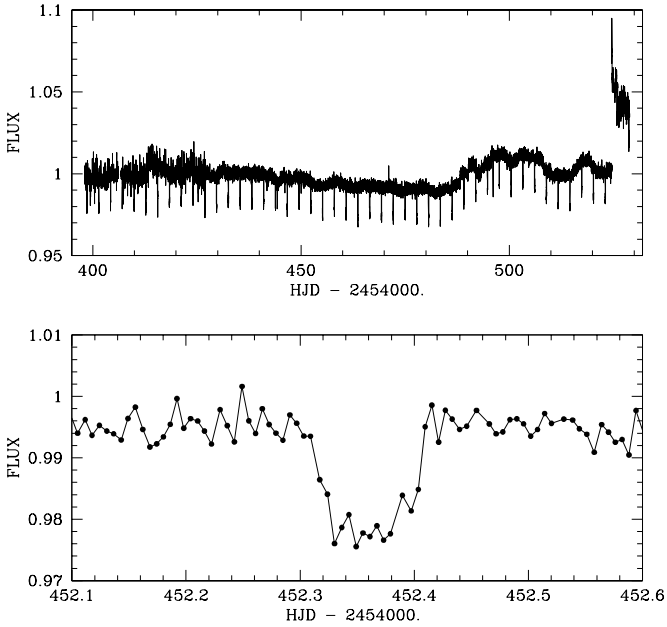

Fig. 1. *Top*: Normalized CoRoT LC of the star CoRoT-12. The oversampled part of the LC was binned to the same time bin than its first part for the sake of clarity. *Bottom*: zoom on a transit of CoRoT-12b.

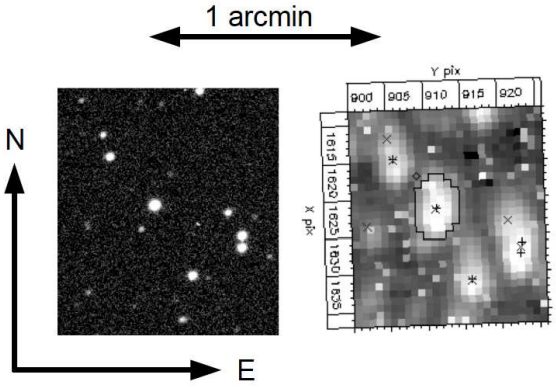

Fig. 2. The sky area around CoRoT-12 (brightest star near the centre). *Left*: *R*-filter image with a resolution of 1.3" taken with the INT/WFC. *Right*: Image taken by CoRoT, at the same scale and orientation. The jagged outline in its center is the photometric aperture mask; indicated are also CoRoT's x and y image coordinates and positions of nearby stars from the Exo-Dat (Deleuil et al 2009) database.

measured flux (more than 5%) caused by the impact of a cosmic ray on the detector can also be noticed in the last part of the LC. The processed LC shown in Fig. 1 has an excellent duty cycle of 91%.

Despite that its CoRoT LC shows some kind of irregular variations with a peak-to-peak amplitude of 2.3%, CoRoT-12 appears to be a photometrically quiet star. Except for the transit signal (see below), the discrete Fourier-transform of the LC shows no clear periodicity over the noise level. The rotational period of the star cannot thus be constrained from the CoRoT photometry.

Periodic transit-like signals are clearly visible in the LC, as can be seen in Fig. 1. Initial values for the orbital period P and transit epoch T_0 were determined by trapezoidal fitting of the transit centers, as described by Alonso et al. (2008). The resulting values were $T_0 = 2545398.6305 \pm 0.0002$ HJD and $P = 2.82805 \pm 0.00005$ days. These values were used to schedule the ground-based follow-up observations (see next Section), and also as initial guesses for the global analysis presented in Sec. 5.

3. Ground-based observations

The following ground-based observations were performed to establish the planetary nature of CoRoT-12b and to better characterize the system.

3.1. Imaging - contamination

CoRoT has a rather poor optical resolution, so performing high-resolution ground-based imaging of its fields is important, not only to assess the possibility that the eclipse signals detected by CoRoT are due to contaminating eclipsing binaries, but also to estimate the dilution of the eclipses measured by CoRoT caused by contaminating stars (see Deeg et al. 2009 for details).

Imaging of the target field was undertaken with the 2.5m INT telescope during pre-launch preparations (Deleuil et al., 2009) and with the IAC80 telescope during candidate follow-up (Deeg et al. 2009). It found no nearby contaminating star that could be a potential false alarm source, i.e. that mimiks CoRoT's signal while being an eclipsing binary star (see Fig. 2).

Using the method describe by Deeg et al. (2009), the fraction of contamination in the CoRoT-12 photometric aperture mask was estimated to be $3.3 \pm 0.5\%$. It is mostly due to a 3.5 mag fainter star that is 8.5" SW. This small dilution was taken into account in our analysis presented in Sec. 5.

3.2. Radial velocities - spectroscopy

Four radial velocity (RV) measurements were obtained with the HARPS spectrograph (Pepe et al. 2002b, Mayor et al. 2003) on the 3.6-m telescope at ESO La Silla Observatory (Chile), on

October 2008 (HARPS program 082.C-0120). These first data were made using the high efficiency mode EGGS in order to establish the planetary nature of the companion, showing a detectable and low-amplitude radial velocity variation in phase with the CoRoT ephemeris, with the shortest exposure time. Ten additionnal measurements were recorded with HARPS, from November 27, 2009 to February 05, 2010 (HARPS program 184.C-0639). These newer data points were acquired using the high accuracy mode HAM to increase the precision of the RV measurements compared to the about 30 m s^{-1} of systematic errors of the high efficiency mode (Moutou et al. 2009), and without simultaneous thorium (obj_AB mode) in order to monitor the Moon background light on the second fiber B.

HARPS HAM and EGGS data were reduced with the on-line standard pipeline except for three of our ten HAM measurements which were strongly contamined by the Moon background light that affected both the RV measurements, in the range between 140 m s^{-1} and 560 m s^{-1}, and the bisector lines. We have corrected these three measurements with a special software correction using Moon spectra simultaneously acquired on the second fiber B (Bonomo et al., in prep.). We could not apply this correction to EGGS observations due to the absence of the fiber B in this mode. However, these EGGS spectra did not need correction because they were observed without the presence of the Moon. Radial velocities were obtained by computing weighted cross-correlation with a numerical G2 mask (Baranne et al. 1996; Pepe et al. 2002a).

Spectra of CoRoT-12 were also acquired with the HIRES spectrograph on the Keck I telescope as part of NASA's key science project in support of the CoRoT mission. A transit was covered by HIRES in January 2009 (ten spectra). Six more HIRES spectra were obtained between December 2009 and January 2010. Differential RVs were computed from these spectra with the *Austral* code (Endl et al. 2000). We noticed that the set-up of the slit decker used in January 2009 did not allow a proper subtraction of the sky background, leading to RV systematics with an amplitude of a few dozens of m.s^{-1}. This set-up was changed for the other HIRES RVs, leading then to a proper background subtraction.

Our HARPS and HIRES measurements are presented in Table 2. An orbital analysis was performed treating the three sets of RV measurements (HARPS HAM, HARPS EGGS, and HIRES) as independent data sets with different zero point velocities, after having zero-weighted the HIRES measurements obtained at the transit phase. The orbital solution was made keeping the period and ephemeris fixed to the CoRoT values, but allowing the zero point offsets to be fit in a least square way. Figure 3 shows the resulting orbital solution which is in phase with the CoRoT photometric signal. The resulting eccentricity (0.03 ± 0.13) was consistent with zero while the semi-amplitude was 124 ± 15 m.s^{-1}. Assuming a solar-mass host star, this semi-amplitude translates into a transiting object with a mass of about 0.9 M_J. In Section 5 we present a revised orbit obtained using a global analysis.

An analysis was made on the residual RVs after removing the orbit to look for the possible presence of additional companions. No significant variations were found, but given the sparseness of the measurements we cannot exclude the presence of additional companions with a good confidence.

The HARPS cross-correlation functions were analyzed using the line-bisector technique (Queloz et al. 2000). No evidence for a clear correlation between the RV variations and the bisector spans was found (Fig. 4), discarding thus the possibility that the periodic signal detected in these RVs is caused by a blended eclipsing binary. Taking into the fact that CoRoT-12 is a solar analog star (see Sect. 4), we interpret thus the eclipses detected in CoRoT photometry as transits of a new giant planet, CoRoT-12b.

HJD (days)	RV (km s^{-1})	σ_{RV} (km s^{-1})	Bisector (km s^{-1})
HARPS EGGS			
2454745.86036	12.1740	0.0221	-0.0256
2454746.83735	11.9341	0.0369	-0.1307
2454747.86641	12.0904	0.0198	-0.0320
2454763.81411	11.9856	0.0121	-0.0435
HARPS HAM			
2455163.73528	12.1193	0.0458	0.0429
2455165.71941	11.9857	0.0263	-0.0310
2455167.72180	12.0570	0.0342	0.0105
2455219.63940	12.0051	0.0195	-0.0111
2455220.68849	12.2435	0.0167	-0.0188
2455226.66329	12.2126	0.0168	0.0246
2455227.68971	12.0348	0.0442	0.0335
2455229.64150	12.2355	0.0292	0.0259
2455231.68894	12.1640	0.0240	0.0167
2455233.60091	11.9993	0.0292	-0.0945
HIRES (transit)			
2454839.77813	0.0080	0.0206	
2454839.78935	-0.0015	0.0067	
2454839.80022	0.0228	0.0154	
2454839.81152	0.0262	0.0092	
2454839.82199	-0.0221	0.0131	
2454839.83296	0.0366	0.0061	
2454839.84351	-0.0562	0.0119	
2454839.85469	-0.0167	0.0090	
2454839.86606	-0.0107	0.0111	
2454839.87681	-0.0242	0.0165	
HIRES (out of transit)			
2455170.99823	-0.0573	0.0286	
2455223.00984	0.0490	0.0144	
2455223.02060	0.0466	0.0144	
2455223.98643	0.1633	0.0143	
2455224.93395	-0.0659	0.0175	
2455224.94528	-0.0979	0.0220	

Table 2. HARPS and HIRES radial velocity measurements for CoRoT-12. The HARPS RVs are absolute, while the HIRES RVs are differential (measured relative to a stellar template). The bisectors were not measured from the HIRES spectra.

4. Stellar parameters

Two master spectra were used to determine the atmospheric parameters of the star. The first of them was made by co-addition of the seven HARPS HAM spectra which were not strongly contamined by the Moon background light. The resulting master spectrum had a signal-to-noise ratio (SNR) about 40 in the continuum. The second master spectrum was obtained from the co-addition of two Keck spectra and had a SNR about 100 in the continuum.

The used methodology was similar to the one described by, e.g., Deleuil et al. (2008). A first estimate of the effective temperature $T_{\rm eff}$ of the star was obtained from the two master spectra using the H_α line profile. For the HARPS master spectrum, we

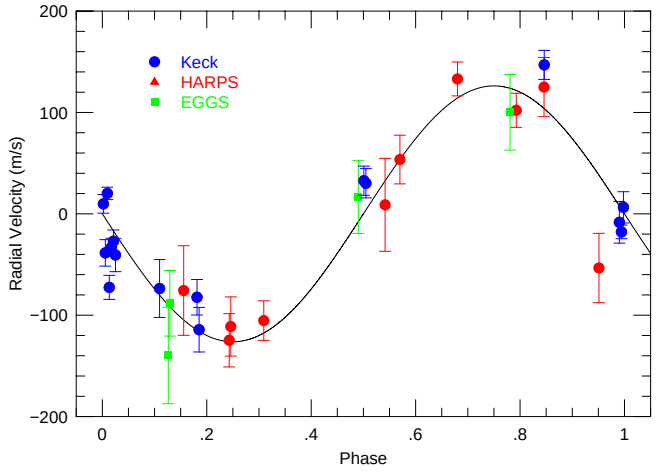

Fig. 3. HARPS and HIRES RVs phase-folded on the CoRoT ephemeris and overimposed on the best fit orbital model.

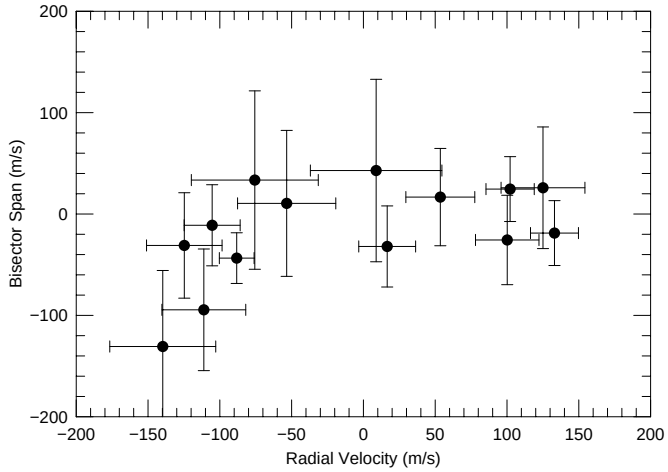

Fig. 4. Bisector versus RV measured from the HARPS spectra. Errors of twice the RV errors were adopted for all the bisector measurements.

used the method described in Bruntt et al. (2004) and based on the division of the stellar H_α profile by that of the Sun observed with the same instrumental configuration. Our best fit value was $T_{\rm eff}$ = 5600 K. For the HIRES spectrum, a classical line profile fitting method yielded a best fit temperature of 5500 K.

A second estimate is based on using the Spectroscopy Made Easy (SME 2.1) package (Valenti & Piskunov 1996, Valenti & Fischer 2005), which uses a grid of stellar models (Kurucz models or MARCS models) to determine the fundamental stellar parameters iteratively. This is achieved by fitting the observed spectrum directly to the synthesized spectrum and minimizing the discrepancies using a non-linear least-squares algorithm. In addition, SME utilises input from the VALD database (Piskunov et al. 1995, Kupka et al. 1999). The uncertainties using SME, as found by Valenti & Fischer (2005), and based on a large sample (of more than 1000 stars) are 44K in $T_{\rm eff}$, 0.06 dex in $\log g$, and 0.03 dex in [M/H] per measurement. However, by comparing the measurements with model isochrones they found a larger, systematic offset of about 0.1 dex and a scatter that can occasionally reach 0.3 dex, in $\log g$. For CoRoT-12, we find an internal discrepancy using SME of 0.1 dex depending on which ion we use to determine $\log g$. We therefore assign 0.1 dex as our 1 σ precision. Here we find a $T_{\rm eff}$ of 5875 K, a $\log g$ of 4.51, an [Fe/H] of +0.21 dex and a $v \sin I$ of 2.9 ± 1 km s^{-1}.

A third estimate and a more careful determination of the abundances is gained by using the semi-automatic package VWA (Bruntt et al. 2002, 2008), which performs iterative fitting of synthetic spectra to reasonably isolated spectral lines, to analyse the HIRES master spectrum. The atmospheric parameters and elemental abundances derived with VWA for CoRoT-12 were considered as our final values and are presented in Table 3.

The Li I line at 670.78 nm was not detected in both master spectra, nor any hint of chromospheric activity. From this, the small rotational velocity measured in the spectra, and the small photometric variability noticed in the CoRoT LC, CoRoT-12 appears thus to be a quiet and slowly rotating solar analog star.

Using $T_{\rm eff}$ and $\log g$ from the VWA spectroscopic analysis, we estimated the absolute magnitude $M_V \simeq 4.75$ mag and colour excess $E(J-K) \simeq 0.08$ mag from the Allen's tables (Cox 2000). We calculated the corresponding interstellar absorption $A_V \simeq 0.46$ (using $A_V = (5.82 \pm 0.1) \times E(J-K)$; Cox 2000), to estimate, with the V apparent magnitude, the distance of the star to be d = 1150 ± 85 pc.

$T_{\rm eff}$	5675 ± 80 K
$\log g$	4.52 ± 0.08
$v_{\rm mic}$	0.6 ± 0.2 km s^{-1}
$v_{\rm mac}$	1.5 ± 0.3 km s^{-1}
$v \sin I$	1.0 ± 1.0 km s^{-1}
d	1150 ± 85 pc
[Fe/H]	0.16 ± 0.10
[Na/H]	0.17 ± 0.06
[Mg/H]	0.13 ± 0.07
[Al/H]	0.15 ± 0.10
[Si/H]	0.12 ± 0.08
[Ca/H]	0.09 ± 0.10
[Sc/H]	0.22 ± 0.15
[Ti/H]	0.05 ± 0.09
[V/H]	0.02 ± 0.08
[Cr/H]	0.17 ± 0.09
[Mn/H]	0.20 ± 0.13
[Co/H]	0.16 ± 0.14
[Ni/H]	0.21 ± 0.08

Table 3. Stellar parameters and elemental abundances derived for CoRoT-12 from our VWA spectroscopic analysis.

5. Global analysis

5.1. Description

We decided to perform a thorough global analysis of the CoRoT transit photometry and HARPS/HIRES RVs to get the strongest constraints on the system parameters. First, we cut the parts of the CoRoT LC located within 0.15 days of the transit mid-times deduced from the preliminary transit ephemeris presented in Sec. 2, getting thus 47 individual transit LCs. Considering their

large number of measurements, we decided to stack the measurements of the 36 over-sampled transit LCs per 4, to speed-up our analysis. This binning did not affect our final precision on the system parameters, as the resulting folded LC (see Fig. 5) is still well sampled.

Our analysis was done with the adaptative Markov Chain Monte-Carlo (MCMC) algorithm presented by Gillon et al. (2009; 2010). MCMC is a Bayesian inference method based on stochastic simulations that samples the posterior probability distributions of adjusted parameters for a given model. Our MCMC implementation uses the Metropolis-Hasting algorithm (see, e.g., Carlin & Louis 2008) to perform this sampling. Our nominal model was based on a star and a transiting planet on a Keplerian orbit about their center of mass. More specifically, we used a classical Keplerian model for the RVs obtained outside the transit, and in addition, a Rossiter-McLaughlin effect model (Giménez, 2006) for the MCMC run using the HIRES data obtained during a transit. To model the eclipse photometry, we used the photometric eclipse model of Mandel & Agol (2002) multiplied by a baseline model consisting of a different fourth-order time polynomium for each of the 47 CoRoT time-series. The coefficients of these baseline models were determined by least-square minimization at each steps of the Markov chains (see Gillon et al. 2010 for details).

Our analysis was composed of a nominal MCMC run, followed by four other MCMC runs having different specificities that are described below and summarized in Table 4. Each of the MCMC runs was composed of five Markov chains of 10^5 steps, the first 20 % of each chain being considered as its burn-in phase and discarded. For each run, the convergence of the five Markov chains was checked using the statistical test presented by Gelman and Rubin (1992).

The correlated noise present in the LCs was taken into account as described by Gillon et al. (2010), i.e., a scaling factor was determined for each LC from the standard deviation of the binned and unbinned residuals of a preliminary MCMC analysis, and it was applied to the error bars (see also Winn et al. 2008). For the RVs, a 'jitter' noise of 5 m.s^{-1} was added quadratically to the error bars, this value being an upper limit for a quiet solar-type star like CoRoT-12 (Wright 2005). Practically, this small jitter noise has no impact on the posterior distributions of the system parameters, as CoRoT-12 is faint and the RV precision is photon noise/background contamination limited. For the four HARPS measurements obtained with the EGGS mode, a systematic error of 30 m.s^{-1} was also added quadratically to the error bars (see Sec. 3.2).

In all five MCMC runs, the following parameters were jump parameters[2]: the planet/star area ratio $(R_p/R_s)^2$, the transit width (from first to last contact) W, the parameter $b' = a\cos i/R_*$ (which is the transit impact parameter in case of a circular orbit), the orbital period P and time of minimum light T_0, the two Lagrangian parameters $e\cos\omega$ and $e\sin\omega$ where e is the orbital eccentricity and ω is the argument of periastron, and the parameter $K_2 = K\sqrt{1-e^2}\,P^{1/3}$, where K is the RV orbital semi-amplitude (see Gillon et al. 2009, 2010). We assumed a uniform prior distribution for all these jump parameters. To take into account the small dilution of the signal due to contaminating stars (see Sec. 3.1), the jump parameters $(R_p/R_s)^2$ was divided at each step of the MCMC by a number drawn from the distribution $N(1.033, 0.005^2)$ before being used in the computation of the eclipse model.

[2] Jump parameters are the parameters that are randomly perturbed at each step of the MCMC.

We did not assume a perfectly circular orbit in any of our MCMC runs despite that a circular orbit is compatible with the results of our orbital analysis of the RVs (see Sec. 3.2). Indeed, most short-period planets could keep a tiny but non-zero eccentricity during a major part of their lifetime (Jackson et al. 2008), so fixing the eccentricity to zero is not justified by tidal theory and could lead to overoptimistic error bars on the system parameters.

Because the bandpass of CoRoT is broad and its transmission peaks at a wavelength for which the effect of the stellar limb-darkening is large, it is important to take into account the influence of the limb-darkening modeling on the precision of the deduced system parameters. We assumed a quadratic limb-darkening law, and we allowed the quadratic coefficients u_1 and u_2 to float in our MCMC runs, using as jump parameters not these coefficients themselves but the combinations $c_1 = 2\times u_1 + u_2$ and $c_2 = u_1 - 2\times u_2$ to minimize the correlation of the obtained uncertainties (Holman et al. 2006). To obtain a limb-darkening solution consistent with theory, we decided to use in our nominal MCMC run (labelled $MCMC_1$ in Table 4) normal prior distributions for u_1 and u_2 based on theoretical values. Sing (2010) presented recently a grid of limb-darkening coefficients specially computed for the CoRoT non-standard bandpass and for several limb-darkening laws. We deduced the values $u_1 = 0.47 \pm 0.03$ and $u_2 = 0.22 \pm 0.02$ from Sing's grid for the spectroscopic parameters of CoRoT-12 and their errors (Table 3). The corresponding normal distributions $N(0.47, 0.03^2)$ and $N(0.22, 0.02^2)$ were used as prior distributions for u_1 and u_2 in our nominal MCMC analysis. To test the impact of these priors on the deduced system parameters, another MCMC run ($MCMC_2$) was performed with different prior distributions for u_1 and u_2 obtained through the following procedure. Theoretical values for u_1 and u_2 and their errors σ_{u_1} and σ_{u_2} were deduced from Claret's tables (2000; 2004) for the V and R filters and the spectroscopic parameters of CoRoT-12b reported in Table 3. As the transmission of CoRoT's bandpass peaks between the V and R transmission maxima, we took as initial values for u_1 and u_2 the mean of the values obtained for both filters. For the errors, we took the mean of the errors deduced for both filters and added it quadratically to the difference between both filters to take into account our ignorance of the effective wavelength of the photometry. We obtained this way the following prior distributions: $u_1 \sim N(0.415, 0.05^2)$ and $u_2 \sim N(0.29, 0.02^2)$. Furthermore, we performed a third MCMC run ($MCMC_3$) assuming a uniform prior distribution for u_1 and u_2 to assess our capacity of constraining the limb-darkening coefficients from the CoRoT photometry alone.

At each step of the Markov chains, the stellar density deduced from the jump parameters, and values for T_{eff} and [Fe/H] drawn from the normal distributions deduced from our spectroscopic analysis, were used as input for the stellar mass calibration law deduced by Torres et al. (2010) from well-constrained detached binary systems[3]. Using the resulting stellar mass, the physical parameters of the system were then deduced from the jump parameters at each MCMC step. To account for the uncertainty on the parameters of the stellar calibration law, the values for these parameters were randomly drawn at each step of the Markov chains from the normal distribution presented by Torres et al. (2010).

[3] The stellar calibration law presented by Torres et al. is in fact function of T_{eff}, [Fe/H] and $\log g$. We modified it to use as input the stellar density instead of the stellar surface gravity (see Anderson et al. 2010b).

In a fourth MCMC run (labelled $MCMC_4$ in Table 4), we also used as data the HIRES RV measurements obtained during a transit of CoRoT-12b. Without any prior knowledge on the actual effect of the background problem on the measured RVs (see Sec. 3.2), we decided to add quadratically a conservative value of 50 m s^{-1} to the error bars. For this run, the parameters $v \sin I \cos\beta$ and $v \sin I \sin\beta$, where $v \sin I$ is the projected rotational speed of the star and β is the projected spin-orbit angle, were also jump parameters in the Markov Chains. A uniform prior distribution was assumed for them, but the normal prior distribution $N(1, 1^2)$ km s^{-1} was used for the deduced parameter $v \sin I$ to get an extra constraint on the posterior distribution of β.

In our fifth MCMC run (labelled $MCMC_5$ in Table 4), we also used as data the parts of the CoRoT LC located within 0.2 days of the *occultation* mid-times deduced from the best fit transit ephemeris of our nominal *MCMC* run. The goal of this run was to obtain an upper limit for the depth of the occultation in the CoRoT photometry. For this run, the occultation depth was thus also a jump parameter.

Finally, we assessed the perfect periodicity of the transits of CoRoT-12b in our sixth run (labelled $MCMC_6$ in Table 4). For this run, a transit timing variation (TTV) was considered as jump parameter for each of the 47 transits. Obviously, the orbital period could not be determined unambiguously without any prior on these TTVs, so we assumed a normal prior distribution centered on zero for each of them. Practically, we added the following Bayesian penalty to our merit function:

$$BP_{\rm timings} = \sum_{i=1,47} \left(\frac{TTV_i}{\sigma_{TT_i}} \right)^2 \quad (1)$$

where TTV_i is the TTV for the i^{th} CoRoT transit, and σ_{TT_i} is the error on its timing estimated by a preliminary individual analysis of this transit.

5.2. Results

Table 5 present the CoRoT-12 system parameters and 1-σ error limits derived from our nominal MCMC run ($MCMC_1$). The results of the five other MCMC runs are presented in Table 6.

Our MCMC analysis presents CoRoT-12b as an inflated Jupiter-mass planet ($M_p = 0.92 \pm 0.07\ M_{Jup}$, $R_p = 1.44 \pm 0.13\ R_{Jup}$) transiting a solar analog star ($M_* = 1.08 \pm 0.08\ M_\odot$, $R_* = 1.1 \pm 0.1\ R_\odot$). Using the stellar density deduced from our MCMC analysis ($\rho_* = 0.77^{+0.20}_{-0.15}\ \rho_\odot$) and the effective temperature and metallicity obtained from spectroscopy (Table 3), a stellar evolution modeling based on the code CLES (Scuflaire et al. 2008) leaded to a stellar mass of $1.07 \pm 0.10\ M_\odot$, in excellent agreement with our MCMC result, and to a poorly constrained age of 6.3 ± 3.1 Gyr. It is also worth noticing that the two independent values obtained for the stellar surface gravity from our spectroscopic and global analysis are in good agreement (1.4 σ), indicating the good coherence of our final solution.

Fig. 6 presents the period-folded CoRoT photometry binned per two minutes time intervals with the best fit transit model superimposed. The standard deviation of the residuals of this latter LC is 592 ppm, demonstrating the excellent quality of the CoRoT photometry.

The results of the first, second and third MCMC runs shows that the limb-darkening coefficients u_1 and u_2 are poorly constrained by the CoRoT transit photometry, despite its good precision. Indeed, the posterior distributions of u_1 and u_2 for the runs $MCMC_1$ and $MCMC_2$ are close to the prior distributions, indicating that the CoRoT data do not constrain much these parameters. This is confirmed by the very broad posterior distributions obtained in the run $MCMC_3$. Fortunately, the posterior distributions for the system parameters obtained in the three runs are in excellent agreement, indicating that the priors chosen for u_1 and u_2 in our nomimal MCMC run does not affect the validity of our results, their only effect being a slight improvement of the precision on the system parameters.

Our final precisions on the stellar and planetary masses and radii are not excellent (about 7% on the masses and about 10% on the radii), and more observations are required to thoroughly characterize this system. In this context, improving significantly the precision on the stellar density (about 20%) is desirable. Such an improvement could be achieved mostly through a better characterization of the orbital parameters $e \cos\omega$ and $e \sin\omega$ with more RV measurements (and possibly occultation photometry). Indeed, an new MCMC analysis assuming a perfectly circular orbit leads > 2 times smaller error bars on the planet's and star's radii. The characterization of the system would also benefit from an improved determination of the transit parameters with more high-precision transit photometry, if possible acquired in a redder bandpass (fainter limb-darkening).

The results of the run $MCMC_4$ show that we cannot constrain the value of the projected spin-orbit angle β from the present data. This is not surprising, considering the small rotational velocity of the star and the large amplitude of the systematic effects present in HIRES transit data taken, as illustrated by Fig. 6. On its side, the run $MCMC_5$ shows that the occultation of the planet is not detected in the CoRoT data. We can only put an upper limit on its depth (3-σ upper limit = 680 ppm).

As expected, the errors on T_0 and P are significantly larger for the run $MCMC_6$, but the posterior distributions obtained for the other parameters agree well with ones of the other MCMC runs. The resulting TTVs are shown in Fig. 7. No transit shows a significant timing variation. Still, the resulting TTV series seems to show a correlated structure. Fitting a sinusoidal function in this series leads to a best-fit period of about 24 epochs , i.e. of about 68 days. Nevertheless, the resulting false alarm probability is high, about 15%, indicating that this correlated structure is not very significant. Still, it is interesting to notice that, if we assume a rotational period of 68 days for the star and $\sin I = 1$, and using $R_* = 1.1\ R_\odot$, we obtain a value of 1.2 km s^{-1} for $v \sin I$, in excellent agreement with the value derived from our spectroscopic analysis (see Table 3). In this context, a possible interpretation of the low-amplitude structure visible in the TTV series is that it is caused by the rotation of the surface of the star and its influence on the transit barycenters.

6. Discussion

The position of CoRoT-12b in a planetary mass-radius diagram is shown in Fig. 7. While being denser than the extremely inflated planets WASP-17b (Anderson et al. 2010a), TrES-4b (Mandushev et al. 2007) and WASP-12b (Hebb et al. 2009), CoRoT-12b appears to be a very low-density 'hot Jupiter'. Using the hypothesis that the planet is a core-less gazeous planet of solar composition, we used the planetary evolution code CEPAN (Guillot & Morel, 1995) to assess the ability of standard irradiated planet models to explain the low-density of CoRoT-12b. Several models were used: a standard model with no extra heat source, a model for which the opacities were artificially multiplied by 30, and three models with a constant energy deposit (10^{26}, 10^{27} and 10^{28} erg.s^{-1}) at the planet's center. Our results in terms of planetary size evolutions are shown in Fig. 9. For recall,

	Data	Jump parameters	Normal prior distributions
$MCMC_1$	CoRoT transits HARPS (EGGS+HAM) HIRES (not transit)	$(R_p/R_s)^2$, W, b', P, T_0, K_2, c_1, c_2, $e\cos\omega$, $e\sin\omega$	$u_1 \sim N(0.47, 0.03^2)$ $u_2 \sim N(0.22, 0.02^2)$
$MCMC_2$	idem $MCMC_1$	idem $MCMC_1$	$u_1 \sim N(0.415, 0.05^2)$ $u_2 \sim N(0.29, 0.02^2)$
$MCMC_3$	idem $MCMC_1$	idem $MCMC_1$	
$MCMC_4$	idem $MCMC_1$ + HIRES transit	idem $MCMC_1$ + $v\sin I\cos\beta$ & $v\sin I\sin\beta$	$u_1 \sim N(0.47, 0.03^2)$ $u_2 \sim N(0.22, 0.02^2)$ $v\sin I \sim N(1, 1^2)$ & > 0 km s^{-1}
$MCMC_5$	idem $MCMC_1$ + CoRoT occultations	idem $MCMC_1$ + occultation depth dF_2	$u_1 \sim N(0.47, 0.03^2)$ $u_2 \sim N(0.22, 0.02^2)$
$MCMC_6$	idem $MCMC_1$	idem $MCMC_1$ + 47 TTVs	$u_1 \sim N(0.47, 0.03^2)$ $u_2 \sim N(0.22, 0.02^2)$ $TTV_{i\in[1:47]} \sim N(0, \sigma^2_{TT,i})$

Table 4. Specificities of the different MCMC runs performed during our global analysis. See text for details

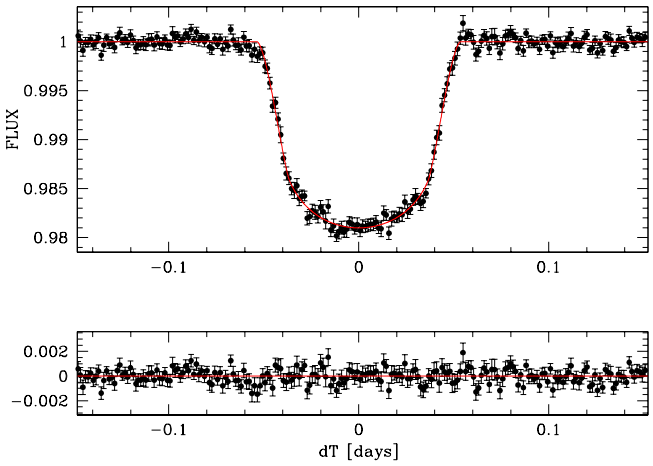

Fig. 5. *Top*: CoRoT transit photometry period-folded and binned per 2 minutes time intervals, with the best fit transit model superimposed. *Bottom*: residuals. Their standard deviation is 592 ppm.

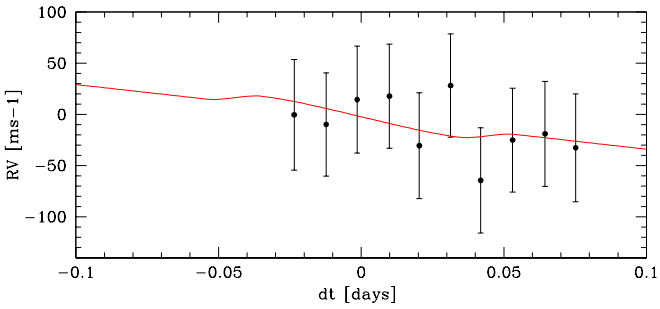

Fig. 6. HIRES RV measurements obtained during a transit of CoRoT-12b, superimposed on an orbital+Rossiter model assuming $v\sin I = 1$ km.s^{-1} and $\beta = 0$ deg. A systematic error of 50 m.s^{-1} was added quadratically to the error bars to take into account the background subtraction problem (see text for details).

we constrain the age of the system to 6.3 ± 3.1 Gyr. Considering this age, the measured size of CoRoT-12b is in good agreement with all four evolution models, and we cannot conclude to an 'anomalously' large radius for CoRoT-12b.

At this point, we can only notice that the hypotheses of an extra heat source and/or of larger opacities are favored by the data, while outlying that a more precise radius measurement is needed to conclude. In this context, it is worth noticing that the precision on the planet's radius is mostly limited by the precision on the orbital eccentricity and argument of periastron (see Sec. 5.2). It is thus desirable to obtain more RV measurements of the system. Better constraining the planet's orbital eccentricity would also make possible the assessment of its past tidal evolution and its influence on its energy budget (e.g., Ibgui et al. 2010).

Acknowledgements. The authors wish to thank the staff at ESO La Silla Observatory for their support and for their contribution to the success of the HARPS project and operation. A part of the data presented herein were obtained at the W.M. Keck Observatory from telescope time allocated to the National Aeronautics and Space Administration through the agency's scientific partnership with the California Institute of Technology and the University of California. The Observatory was made possible by the generous financial support of the W.M. Keck Foundation. The authors wish to recognize and acknowledge the very significant cultural role and reverence that the summit of Mauna Kea has always had within the indigenous Hawaiian community. We are most fortunate to have the opportunity to conduct observations from this mountain. The team at IAC acknowledges support by grant ESP2007-65480-C02-02 of the Spanish Ministerio de Ciencia e Innovación. The building of the input CoRoT/Exoplanet catalog (Exo-dat) was made possible thanks to observations collected for years at the Isaac Newton Telescope (INT), operated on the island of La Palma by the Isaac Newton group in the Spanish Observatorio del Roque de Los Muchachos of the Instituto de Astrophysica de Canarias. The German CoRoT team (TLS and University of Cologne) acknowledges DLR grants 50OW0204, 50OW0603, and 50QP07011. The French team wish to thank the "Programme National de Planétologie" (PNP) of CNRS/INSU and the French National Research Agency (ANR-08-JCJC-0102-01) for their continuous support to our planet search. The Swiss team acknowledges the ESA PRODEX program and the Swiss National Science Fundation for their continuous support on CoRoT ground follow-up. M. Gillon acknowledges support from the Belgian Science Policy Office in the form of a Return Grant, and thanks B.-O. Demory for usefull discussions.

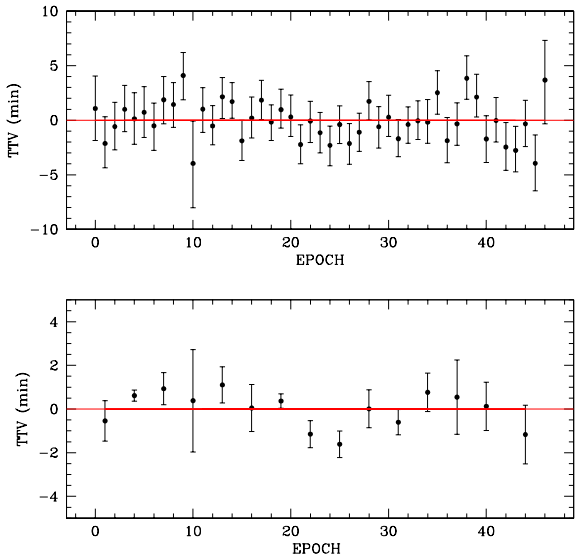

Fig. 7. *Top*: median value and 1-σ limits of the TTV posterior distributions obtained in $MCMC_6$. *Bottom*: same curve obtained after binning the TTVs per three (error of each bin = error on the mean).

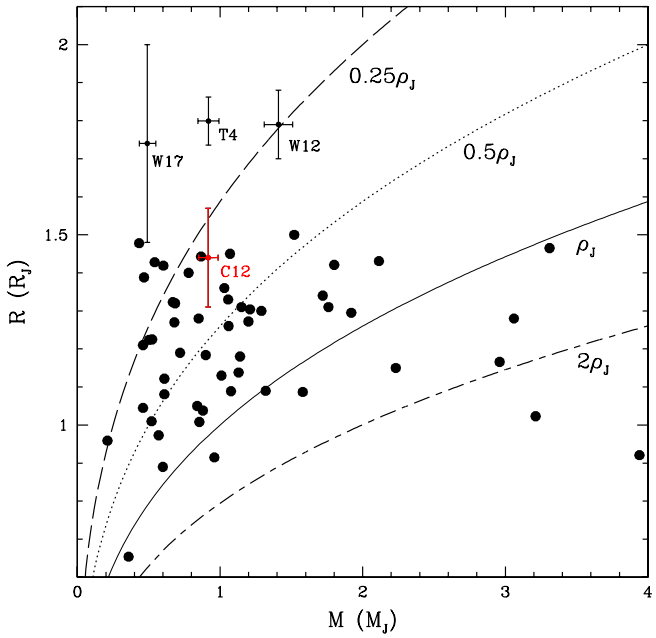

Fig. 8. Position of CoRoT-12b (in red) among the other transiting planets (black circles, values from http://exoplanet.eu) in a mass-radius diagram. The error bars are shown only for CoRoT-12b (C12), WASP-17b (W17), TrES-4b (T4), and WASP-12b (W12) for the sake of clarity.

Parameter	Posterior distribution (median + 1-σ limits)
Jump parameters	
Planet/star area ratio $(R_p/R_s)^2$	$0.01744^{+0.00039}_{-0.00040}$
$b' = a\cos i/R_*$ [R_*]	$0.609^{+0.055}_{-0.057}$
Transit width W [d]	$0.10726^{+0.00089}_{-0.00090}$
Transit epoch $T_0 - 2450000$ [HJD]	4398.62707 ± 0.00036
Orbital period P [d]	2.828042 ± 0.000013
RV K_2 [m.s^{-1}.d$^{1/3}$]	177^{+12}_{-11}
$e\cos\omega$	$-0.012^{+0.024}_{-0.028}$
$e\sin\omega$	$0.053^{+0.073}_{-0.066}$
c_1	1.152 ± 0.056
c_2	0.028 ± 0.052
Deduced stellar parameters	
u_1	0.466 ± 0.027
u_2	0.219 ± 0.021
Stellar density ρ_* [$\rho_\odot$]	$0.77^{+0.20}_{-0.15}$
Stellar surface gravity $\log g_*$ [cgs]	$4.375^{+0.065}_{-0.062}$
Stellar mass M_* [$M_\odot$]	$1.078^{+0.077}_{-0.072}$
Stellar radius R_* [$R_\odot$]	$1.116^{+0.096}_{-0.092}$
Deduced planet parameters	
RV K [m s^{-1}]	$125.5^{+8.0}_{-7.5}$
$b_{transit}$ [R_*]	$0.573^{+0.027}_{-0.030}$
$b_{occultation}$ [R_*]	$0.64^{+0.10}_{-0.09}$
$T_{occultation} - 2450000$ [HJD]	$4400.020^{+0.055}_{-0.052}$
Orbital semi-major axis a [AU]	$0.04016^{+0.00093}_{-0.00092}$
Orbital inclination i [deg]	$85.48^{+0.72}_{-0.77}$
Orbital eccentricity e	$0.070^{+0.063}_{-0.042}$
Argument of periastron ω [deg]	105^{+90}_{-27}
Planet equilibrium temperature T_{eq} [K] [a]	1442 ± 58
Planet density ρ_p [ρ_{Jup}]	$0.309^{+0.097}_{-0.071}$
Planet surface gravity $\log g_p$ [cgs]	$3.043^{+0.082}_{-0.080}$
Planet mass M_p [M_J]	$0.917^{+0.070}_{-0.065}$
Planet radius R_p [R_J]	1.44 ± 0.13

Table 5. Median and 1-σ limits of the posterior distributions obtained for the CoRoT-12 system from our global analysis. These results were obtained in our first MCMC run (see Sec. 5 for details). [a]Assuming A=0 and F=1.

References

Alonso R., Auvergne M., Baglin A., et al., 2008, A&A, 482, L21
Anderson D. R., Hellier C., Gillon M., et al., 2010, ApJ, 709, 159
Anderson D. R., Gillon M., Maxted P. F. L., et al., 2010, A&A, 513, L3
Auvergne M., Bodin P., Boisnard L., et al., 2009, A&A, 506, 411
Baglin A., Auvergne M., Barge P., et al., 2009, *Transiting Planets*, Proceedings of the International Astronomical Union, IAU Symposium, 253, 71
Baranne, A., Queloz, D., Mayor, M., et al. 1996, A&AS, 119, 373
Barge P., Baglin A., Auvergne M., et al., 2008, A&A, 482, L17
Bruntt H.,Catala C., Garrido R., et al., 2002, A&A, 389, 345
Bruntt H., Bikmaev I. F., Catala C., et al., 2004, A&A, 425, 683
Bruntt H., De Cat P., Aerts C., 2008, A&A, 478, 487
Carlin B. P., Louis T. A., 2008, *Bayesian Methods for Data Analysis*, Third Edition (Chapman & Hall/CRC)
Claret A., 2000, A&A, 363, 1081
Claret A., 2004, A&A, 428, 1001
Cox A. N., 2000, Allen's Astrophysical Quantities, AIP Press, Springer
Deeg H. J., Gillon M., Shporer A., et al., 2009, A&A, 506, 343
Deeg H. J., Moutou C., Eriksson A., et al., 2010, Nature, 464, 384
Deleuil M., Deeg H. J., Alonso R., et al., 2008, A&A, 491, 889
Deleuil M., Meunier J. C., Moutou C., et al., 2009, AJ, 138, 649
Deming D., Seager S., 2009, Nature, 462, 302
Endl M., Kürster M., Els S., 2000, A&A, 363, 585
Gelman A., Rubin D., 1992, Statistical Science, 7, 457
Gillon M., Demory B.-O., Triaud A. H. M. J., et al., 2009, A&A, 506, 359
Gillon M., Lanotte A. A., Barman T., et al., 2010, A&A, 511, 3
Giménez A., 2006, ApJ, 650, 408
Guillot T., Morel P., 1995, A&AS, 109, 109

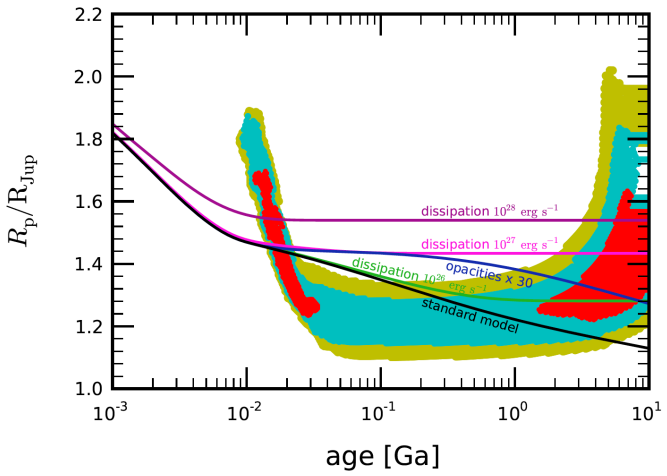

Fig. 9. Evolution of the size of CoRoT-12b (in Jupiter units, R_{Jup}) as a function of age (in billion years), compared to constraints inferred from CoRoT photometry, spectroscopy, radial velocimetry and CESAM stellar evolution models. Red, blue and yellow-green dots correspond to the planetary radii and ages that result from stellar evolution models matching the inferred $\rho_* T_{\rm eff}$ uncertainty ellipse within 1σ, 2σ and 3σ, respectively. Planetary evolution models for a planet with a solar-composition envelope and no core are shown as plain lines and are labeled as follow : *standard (black)*: irradiated planet with no extra heat source ; *opacities x 30 (blue)*: opacities have been artificially multiplied by 30 compared to standard model ; *dissipation*: models in which 10^{26} (*green*), 10^{27} (*pink*), and 10^{28} (*purple*) erg s^{-1} is deposited at the planet's center. These models assume a total mass of 0.92 M_{Jup} and an equilibrium temperature of 1450 K

Hebb L., Collier-Cameron A., Loeillet B., et al., 2009, ApJ, 693, 1920
Holman M. J., Winn J. N., Latham D. W., et al., 2006, ApJ, 652, 1715
Ibgui L., Burrows A., Spiegel D. S., 2010, ApJ, 713, 751
Jackson B., Greenberg R., Barnes R., 2008, ApJ, 681, 1631
Kupka F., Piskunov N., Ryabchikova T. A., et al., 1999, A&AS, 138, 119
Léger, A., Rouan, D., Schneider, J., et al., 2009, A&A, 506, 287
Mandel K., Agol E., 2002, ApJ, 580, 171
Mandushev G., ODonovan F. T., Charbonneau D., et al., 2007, ApJ, 667, L195
Mayor, M., Pepe, F., Queloz, D., et al., 2003, The Messenger, 114, 20
Moutou C., Pont F., Bouchy F., et al., 2009, A&A, 506, 321
Pepe, F., Mayor, M., Galland, F., et al. 2002a, A&A, 388, 632
Pepe, F., Mayor, M., Rupprecht, G., et al. 2002b, The Messenger, 110, 9
Piskunov N. E., Kupka F., Ryabchikova T. A., et al., 1995, A&AS, 112, 525
Queloz D., Eggenberger A., Mayor M., et al., 2000, A&A, 359, L13
Queloz D., Bouchy F., Moutou C., et al., 2009, A&A, 506, 303
Rauer H., Queloz D., Csizmadia Sz, et al., 2009, A&A, 506, 281
Scuflaire R., Théado S., Montalbán J., et al., APSS, 316, 83
Sing D. K., 2010, A&A, 510, 21
Skrustkie M. F., Cutri R. M., Stiening M. D., et al., 2006, AJ, 131, 1163
Surace C., Alonso R., Barge P., et al., 2008, Proceedings of the SPIE, Volume 7019
Torres G., Andersen J., Giménez A., 2010, A&ARv, 18, 67
Valenti J. A., Piskunov N., 1996, A&AS, 118, 595
Valenti J. A., Fischer D. A., 2005, ApJS, 159, 141
Winn J. N., Holman M. J., Torres T., et al., 2008, ApJ, 683, 1076
Winn J. N., 2010, to appear in *Exoplanets*, S. Seager (eds.), University of Arizona Press, Tucson, arXiv:1001.2010
Wright J. T., 2005, PASP, 117, 657

[1] Université de Liège, Allée du 6 août 17, Sart Tilman, Liège 1, Belgium
[2] Thüringer Landessternwarte, Sternwarte 5, Tautenburg 5, D-07778 Tautenburg, Germany
[3] Institute of Planetary Research, German Aerospace Center, Rutherfordstrasse 2, 12489 Berlin, Germany
[4] Research and Scientic Support Department, ESTEC/ESA, PO Box 299, 2200 AG Noordwijk, The Netherlands
[5] Laboratoire d'Astrophysique de Marseille, 38 rue Frédéric Joliot-Curie, 13388 Marseille cedex 13, France
[6] Department of Physics, Denys Wilkinson Building Keble Road, Oxford, OX1 3RH
[7] Observatoire de l'Université de Genève, 51 chemin des Maillettes, 1290 Sauverny, Switzerland
[8] LESIA, Observatoire de Paris, Place J. Janssen, 92195 Meudon cedex, France
[9] Department of Physics and Astronomy, University of Canterbury, Private Bag 4800, Christchurch 8140, New Zealand
[10] Institut d'Astrophysique Spatiale, Université Paris-Sud 11 & CNRS (UMR 8617), Bât. 121, 91405 Orsay, France
[11] Observatoire de Haute Provence, 04670 Saint Michel l'Observatoire, France
[12] Institut d'Astrophysique de Paris, UMR7095 CNRS, Université Pierre & Marie Curie, 98bis boulevard Arago, 75014 Paris, France
[13] LUTH, Observatoire de Paris, CNRS, Université Paris Diderot, 5 place Jules Janssen, 92195 Meudon, France
[14] Rheinisches Institut für Umweltforschung an der Universität zu Köln, Aachener Strasse 209, 50931, Germany
[15] McDonald Observatory, The University of Texas at Austin, Austin, TX 78731, USA
[16] Instituto de Astrofísica de Canarias, E-38205 La Laguna, Tenerife, Spain
[17] University of Vienna, Institute of Astronomy, Türkenschanzstr. 17, A-1180 Vienna, Austria
[18] IAG-Universidade de Sao Paulo, Brazil
[19] Université de Nice-Sophia Antipolis, CNRS UMR 6202, Observatoire de la Côte d'Azur, BP 4229, 06304 Nice Cedex 4, France
[20] Space Research Institute, Austrian Academy of Science, Schmiedlstr. 6, A-8042 Graz, Austria
[21] School of Physics and Astronomy, Raymond and Beverly Sackler Faculty of Exact Sciences, Tel Aviv University, Tel Aviv, Israel
[22] Center for Astronomy and Astrophysics, TU Berlin, Hardenbergstr. 36, 10623 Berlin, Germany

Parameter	$MCMC_2$	$MCMC_3$	$MCMC_4$	$MCMC_5$	$MCMC_6$
Jump parameters					
Planet/star area ratio $(R_p/R_s)^2$	$0.01737^{+0.00041}_{-0.00039}$	$0.01737^{+0.00066}_{-0.00068}$	$0.01749^{+0.00048}_{-0.00042}$	$0.01739^{+0.00044}_{-0.00041}$	$0.01735^{+0.00044}_{-0.00043}$
$b' = a\cos i/R_*$ [R_*]	$0.588^{+0.076}_{-0.051}$	$0.588^{+0.071}_{-0.055}$	$0.613^{+0.068}_{-0.061}$	$0.614^{+0.060}_{-0.056}$	$0.592^{+0.040}_{-0.046}$
Transit width W [d]	0.1074 ± 0.0010	$0.1077^{+0.0017}_{-0.0013}$	0.1075 ± 0.0011	$0.1071^{+0.0013}_{-0.0011}$	$0.1071^{+0.0011}_{-0.0013}$
$T_0 - 2450000$ [HJD]	$4398.62714^{+0.00032}_{-0.00038}$	$4398.62711^{+0.00041}_{-0.00039}$	$4398.62712^{+0.00040}_{-0.00036}$	$4398.62704^{+0.00038}_{-0.00036}$	$4398.6266^{+0.0013}_{-0.0012}$
Orbital period P [d]	$2.828039^{+0.000014}_{-0.000012}$	2.828040 ± 0.000015	$2.828039^{+0.000014}_{-0.000013}$	$2.828043^{+0.000013}_{-0.000014}$	$2.828061^{+0.000052}_{-0.000047}$
RV K_2 [$m.s^{-1}.d^{1/3}$]	177 ± 11	179 ± 11	177 ± 11	176 ± 11	177 ± 10
$e\cos\omega$	$-0.011^{+0.022}_{-0.023}$	$-0.009^{+0.022}_{-0.024}$	$-0.010^{+0.025}_{-0.029}$	$0.000^{+0.020}_{-0.040}$	$-0.017^{+0.024}_{-0.026}$
$e\sin\omega$	$0.032^{+0.078}_{-0.069}$	$0.023^{+0.074}_{-0.060}$	$0.058^{+0.073}_{-0.079}$	$0.069^{+0.069}_{-0.082}$	$0.043^{+0.072}_{-0.053}$
c_1	$1.121^{+0.077}_{-0.082}$	$1.14^{+0.13}_{-0.15}$	$1.156^{+0.057}_{-0.054}$	$1.153^{+0.054}_{-0.059}$	$1.146^{+0.058}_{-0.050}$
c_2	-0.164 ± 0.059	$-0.4^{+1.1}_{-0.9}$	$0.033^{+0.049}_{-0.054}$	$0.031^{+0.052}_{-0.051}$	$0.027^{+0.048}_{-0.049}$
$v\sin I\cos\beta$ [$km\,s^{-1}$]			-0.1 ± 1.4		
$v\sin I\sin\beta$ [$km\,s^{-1}$]			0.2 ± 1.4		
dF_2				$0.00009^{+0.00022}_{-0.00009}$	
Deduced stellar parameters					
u_1	$0.416^{+0.038}_{-0.041}$	$0.38^{+0.24}_{-0.20}$	$0.469^{+0.027}_{-0.028}$	$0.468^{+0.026}_{-0.029}$	$0.464^{+0.028}_{-0.025}$
u_2	$0.290^{+0.020}_{-0.021}$	$0.36^{+0.35}_{-0.40}$	0.218 ± 0.020	0.217 ± 0.020	$0.219^{+0.020}_{-0.019}$
Density ρ_* [$\rho_\odot$]	0.84 ± 0.21	0.85 ± 0.19	$0.77^{+0.22}_{-0.17}$	$0.75^{+0.20}_{-0.15}$	$0.81^{+0.18}_{-0.12}$
Surface gravity $\log g_*$ [cgs]	$4.396^{+0.064}_{-0.078}$	$4.399^{+0.056}_{-0.072}$	4.372 ± 0.071	$4.366^{+0.066}_{-0.063}$	$4.388^{+0.055}_{-0.046}$
Mass M_* [$M_\odot$]	$1.074^{+0.078}_{-0.071}$	$1.074^{+0.078}_{-0.072}$	$1.081^{+0.077}_{-0.074}$	$1.083^{+0.075}_{-0.074}$	$1.076^{+0.077}_{-0.071}$
Radius R_* [$R_\odot$]	$1.09^{+0.12}_{-0.09}$	$1.08^{+0.11}_{-0.08}$	$1.12^{+0.11}_{-0.10}$	$1.129^{+0.097}_{-0.092}$	$1.098^{+0.072}_{-0.076}$
$v\sin I$ [$km\,s^{-1}$]			$1.67^{+0.87}_{-0.78}$		
Deduced planet parameters					
RV K [$m\,s^{-1}$]	126.0 ± 7.6	$126.6^{+7.9}_{-7.6}$	$125.6^{+8.0}_{-7.6}$	$125.4^{+7.4}_{-7.7}$	125.5 ± 7.1
$b_{transit}$ [R_*]	$0.574^{+0.031}_{-0.036}$	$0.578^{+0.036}_{-0.048}$	$0.578^{+0.033}_{-0.031}$	$0.571^{+0.031}_{-0.033}$	$0.564^{+0.033}_{-0.038}$
$b_{occultation}$ [R_*]	$0.60^{+0.13}_{-0.08}$	$0.60^{+0.12}_{-0.08}$	$0.64^{+0.13}_{-0.10}$	$0.65^{+0.11}_{-0.09}$	$0.620^{+0.071}_{-0.078}$
$T_{occultation} - 2450000$ [HJD]	$4400.021^{+0.040}_{-0.041}$	$4400.025^{+0.040}_{-0.044}$	$4400.023^{+0.045}_{-0.052}$	$4400.041^{+0.036}_{-0.073}$	$4400.010^{+0.043}_{-0.048}$
Orbital semi-major axis a [AU]	$0.04011^{+0.00095}_{-0.00090}$	$0.04011^{+0.00094}_{-0.00092}$	$0.04020^{+0.00093}_{-0.00094}$	$0.04022^{+0.00091}_{-0.00093}$	$0.04013^{+0.00094}_{-0.00090}$
β [deg]			224^{+142}_{-114}		
Orbital inclination i [deg]	$85.8^{+0.6}_{-1.0}$	$85.76^{+0.61}_{-0.93}$	$85.43^{+0.78}_{-0.93}$	$85.39^{+0.72}_{-0.84}$	$85.67^{+0.59}_{-0.51}$
Orbital eccentricity e	$0.059^{+0.057}_{-0.034}$	$0.054^{+0.051}_{-0.031}$	$0.077^{+0.061}_{-0.049}$	$0.083^{+0.062}_{-0.047}$	$0.059^{+0.061}_{-0.031}$
Argument of periastron ω [deg]	109^{+134}_{-31}	112^{+143}_{-36}	112^{+163}_{-23}	87^{+33}_{-88}	113^{+92}_{-26}
Equilibrium temperature T_{eq} [K][a]	1425^{+70}_{-60}	1424^{+63}_{-52}	1446^{+66}_{-63}	1449^{+60}_{-58}	1431 ± 47
Density ρ_p [ρ_{Jup}]	0.34 ± 0.10	$0.342^{+0.099}_{-0.092}$	$0.30^{+0.11}_{-0.08}$	$0.298^{+0.093}_{-0.069}$	$0.327^{+0.082}_{-0.058}$
Surface gravity $\log g_p$ [cgs]	$3.069^{+0.082}_{-0.096}$	$3.073^{+0.077}_{-0.092}$	$3.037^{+0.091}_{-0.089}$	$3.031^{+0.083}_{-0.077}$	$3.060^{+0.065}_{-0.063}$
Mass M_p [M_{Jup}]	$0.919^{+0.068}_{-0.067}$	$0.924^{+0.070}_{-0.067}$	$0.919^{+0.072}_{-0.066}$	$0.916^{+0.068}_{-0.064}$	$0.915^{+0.068}_{-0.064}$
Radius R_p [R_{Jup}]	$1.39^{+0.16}_{-0.12}$	$1.39^{+0.15}_{-0.11}$	$1.45^{+0.15}_{-0.14}$	$1.45^{+0.13}_{-0.12}$	$1.41^{+0.10}_{-0.09}$

Table 6. Median and 1-σ limits of the posterior distributions obtained for the CoRoT-12 system derived from the MCMC runs $MCMC_2$, $MCMC_3$, $MCMC_4$, $MCMC_5$, and $MCMC_6$ (see Table 4). [a]Assuming A=0 and F=1.